Vibronic coupling in indole: I. Theoretical description of the ^1L_a–^1L_b interaction and the electronic spectrum†

Christian Brand,[a] Jochen Küpper,[b] David W. Pratt,[c] W. Leo Meerts,[d] Daniel Krügler,‡[a] Jörg Tatchen[a] and Michael Schmitt*[a]

Received 26th January 2010, Accepted 20th March 2010
First published as an Advance Article on the web 21st April 2010
DOI: 10.1039/c001776k

The properties of the three lowest singlet electronic states (ground, ^1L_b, and ^1L_a states) of indole (C_8H_7N) have been calculated with second-order approximate coupled-cluster theory (CC2) within the resolution-of-the-identity approximation. Refined electronic energies at the CC2 optimized structures and transition dipole moments were calculated using a density functional theory multi-reference configuration-interaction (DFT/MRCI) approach. Structures, energies, and dipole moments are reported for all three states and compared to experimental values. From the optimized structures and calculated transition dipole moments, we predict that pure ^1L_b bands will have positive signs for both the axis reorientation angle θ_T and the angle θ of the transition dipole moment with respect to the inertial a axis. For ^1L_a bands the signs of both angles will be reversed. Vibronically coupled bands can exhibit opposite signs for θ and θ_T. The absorption and emission spectra of indole are calculated based on the Franck–Condon Herzberg–Teller approximation using numerical transition dipole moment derivatives at the DFT/MRCI level of theory. Implications for the experimentally observed vibronic spectra are discussed. Predictions are made for rotationally resolved spectra of various rovibronic bands. A conical intersection, connecting the ^1L_b and ^1L_a states, which can be accessed to varying extents *via* different Herzberg–Teller active modes is found approximately 2000 cm^{-1} above the ^1L_b minimum.

1. Introduction

Indole, the chromophore of tryptophan, has attracted much attention because of its role as a fluorescence marker in biological systems.[1–5] This is partly due to the environmentally sensitive intensity changes of tryptophan fluorescence, which have been extensively used in the study of proteins.[6,7] Currently, it is known from measurements of the electronic absorption spectrum of the isolated molecule in molecular beams that the first excited electronic state of indole is the ^1L_b state, primarily because the transition moment of the lowest energy electronic origin band makes a large positive angle ($+38^\circ$) with respect to the long axis. Similar results, though less precise, have been obtained from linear dichroism measurements on partially oriented molecules in stretched polyethylene films.[8] The ^1L_a state, on the other hand, exhibits a transition dipole moment direction that makes a large negative angle with the long axis. Despite many efforts, all previous attempts to locate the origin of this state in the isolated molecule have failed, though it is still possible that the emitting state in the condensed phase is the ^1L_a.

Recently we have discovered that some of the higher energy vibronic bands in the absorption spectrum of the isolated molecule exhibit negative transition moment angles and positive axis reorientation angles (see Ref. 9). Clearly, these bands have ^1L_a character. One or another of these bands might be the true ^1L_a origin. But it is also possible that these bands are ^1L_b bands, and gain their oscillator strength (and transition moment orientations) by vibronic coupling with the ^1L_a state. The fact that this behavior is not monotonic in the energy above the origin of the ^1L_b state, and therefore might be mode-selective, supports (but does not prove) the vibronic coupling argument.

Motivated by these experimental findings, we have developed a full *ab initio* description of the photophysics of the three lowest singlet states of indole. Here, we want to address especially the location of the ^1L_a state, the role of Herzberg–Teller (HT) coupling[10] in the vibronic spectrum, and the determination of the conical intersection that connects the bound ^1L_a and ^1L_b states.§

[a] *Heinrich-Heine-Universität, Institut für Physikalische Chemie I, 40225 Düsseldorf, Germany. E-mail: mschmitt@uni-duesseldorf.de*
[b] *Fritz-Haber-Institut der Max-Planck-Gesellschaft, 14165 Berlin, Germany*
[c] *University of Pittsburgh, Department of Chemistry, Pittsburgh, PA 15260, USA*
[d] *Radboud University Nijmegen, Institute for Molecules and Materials, Heyendaalseweg 135, NL-6525 AJ Nijmegen, The Netherlands*

† Electronic supplementary information (ESI) available: The Cartesian coordinates (in Å) for all optimized structures of indole at the CC2 level with the cc-pVTZ basis set, the Molden files, containing the vibrational spectrum for all optimized structures and the Gaussian log file containing the optimization of the structure of the conical intersection at the (10,9)-CASSCF level of theory with the 6-311G(d,p) basis set. See DOI: 10.1039/c001776k

‡ Present address: Bruker-Daltonik GmbH, 28359 Bremen, Germany.

§ It should be pointed out that for molecules without at least C_{2v} symmetry the notations "^1L_a" and "^1L_b" are not based on symmetry arguments and in fact in the C_s case, as for indole, they belong to states with the same symmetry. These labels are merely a historic and convenient naming convention[11] to specify the lowest excited electronic states.

Several spectroscopic properties allow for a distinction of ^1L_a and ^1L_b character of the vibronic transitions.[8,12–17] These include the intensities in two-photon excitation experiments, the direction of the transition dipole moment from rotationally resolved electronic spectra, the magnitude and direction of the excited state dipole moments from Stark experiments, and solvatochromic shifts in polar and nonpolar solvents. For example, Sammeth *et al.*[12] proposed that the electronic origin intensity of the ^1L_a state is shared between two bands at 455 and 480 cm^{-1} above the ^1L_b origin. This assignment was rejected based on a vibronic analysis and the bands at 455 and 480 cm^{-1} were reinterpreted as a Fermi doublet.[14] A site-selective investigation of the electronic states of indole in an argon matrix gave further proof to this assumption and located the true ^1L_a origin at about 1400 cm^{-1} above the ^1L_b origin.[15] But the exact location of the electronic origin of the ^1L_a state is still unknown.

Theoretically, the crossing of the ^1L_a and ^1L_b states was investigated by Callis[18] using the semiempirical intermediate neglect of differential overlap configuration interaction (INDO/S-CI) method. From the calculated π-orbital density differences he identified the double bond stretch as the primary internal tuning mode for the ^1L_a–^1L_b conical intersection in indole. This work was extended by Slater and Callis using CIS and CIS-MP2 treatment for the excited states.[19] They used a 29-dimensional vector of planar internal coordinates connecting the corresponding ^1L_a and ^1L_b minima (the so-called ^1L_a–^1L_b difference vector). Along this path both electronic states show an avoided crossing with an energy gap of about 100 cm^{-1}. Later on, the vibronic spectrum of indole was computed in the Franck–Condon (FC) approximation.[1] The general appearance of the spectrum was well reproduced, but features that were attributed to Herzberg–Teller (HT) coupling of ^1L_b levels to the ^1L_a state, such as the intensities of the 28_0^1 or 14_0^1 bands, showed considerable deviations from experiment. Theoretical electronic absorption and emission spectra of indole in the gas phase and in solvents were calculated using complete-active-space self-consistent-field (CASSCF) theory and its extension with second-order perturbation theory corrections (CASPT2).[2–4]

In *ab initio* investigations of the photophysics of indole the potential energy profile of the lowest πσ* state along the NH stretching coordinate was calculated.[5] The πσ* state crosses both the ^1L_a and ^1L_b states as well as the electronic ground state along this coordinate, providing an efficient mechanism for internal conversion. The importance of this relaxation channel has been experimentally proven using photofragment translational spectroscopy.[20]

A thorough investigation of the vibrational structure of the excited states of indole requires the inclusion of HT terms. How such calculations may be performed for multidimensional systems within the harmonic approximation including Dushinsky effects has been shown *e.g.* by Berger *et al.* for benzene and pyrazine.[21] Recently Böhm *et al.* presented an analysis of the vibronic spectrum of tryptamine using Franck–Condon–Herzberg–Teller (FCHT) theory.[22] Here, we present the result of a vibronic analysis of the lowest electronic transitions of indole using HT theory, with density functional theory multi-reference configuration-interaction (DFT/MRCI) computed derivatives of the transition dipole moment with respect to the normal coordinates. The geometries, energies, dipole moments, transition properties and conical intersections of the lowest ππ* states are discussed. In the following paper[9] we will compare these results to the findings of rotationally resolved electronic excitation spectroscopy on several vibronic bands of indole.

2. Computational methods

Structure optimizations were performed employing Dunning's correlation consistent basis sets of valence triple ζ quality (cc-pVTZ)[23] from the TURBOMOLE library.[24] The equilibrium geometries of the electronic ground and the lowest excited singlet states were optimized at the CC2 level within the resolution-of-the-identity approximation[25–27] using the appropriate triple ζ auxiliary basis sets.[28] Ground-state and excited-state vibrational frequencies were calculated using numerical derivatives of analytic gradients using the NumForce script.

The conical intersection (CI) of the ^1L_a and ^1L_b states has been optimized at the (10,9)-CASSCF level of theory with the 6-311G(d,p) basis set using the Gaussian03 program package[29] with the direct algorithm for location of the lowest energy point on a potential surface crossing.[30]

Transition dipole moments for the FCHT analysis were calculated using the combined density functional theory multi-reference configuration interaction (DFT/MRCI) method.[31] The configuration state functions (CSFs) in the MRCI expansion are constructed from Kohn–Sham (KS) orbitals, optimized for the dominant closed shell determinant of the electronic ground state employing the BH-LYP functional.[32,33] All valence electrons were correlated in the MRCI runs. The lowest five roots in the singlet manifold were calculated. The initial set of CSFs was generated from all single and double excitations out of the five highest occupied molecular orbitals in the KS determinant into the five lowest virtual orbitals and was then iteratively improved. The MRCI expansion was kept moderate by extensive configuration selection. The selection of the most important CSFs was based on an energy gap criterion.[31] Only those configurations were taken into account whose energy did not exceed a certain cutoff energy. The energy of a given configuration was estimated from orbital energies within the selection procedure. The cutoff energy was given by the energy of the highest desired root as calculated for the reference space plus a cutoff parameter $\delta E_{sel} = 1.0\ E_H$. This choice has been shown to yield well converged results in practice.[31]

Derivatives of the electronic dipole transition moment with respect to normal coordinates were calculated numerically using central finite differences both at the DFT/MRCI and CC2 levels of theory.

3. Results and discussion

3.1 Optimized geometries of the ^1L_b and ^1L_a states

Table 1 summarizes the ground-state heavy-atom structure of indole at the CC2/cc-pVTZ level of theory, and the excited-state

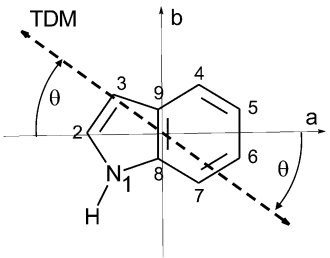

Fig. 1 Atomic numbering and definition of the transition dipole moment orientation angle θ in the plane of the molecule.

heavy-atom structures of the ^1L_a and the ^1L_b states as changes of bond lengths with respect to the ground-state values. The corresponding atomic numbering is given in Fig. 1. Cartesian coordinates for all calculated structures are provided in the ESI.† In Table 1, our calculated geometry changes upon electronic excitation are also compared to values from CASSCF optimized structures.[2]

While the structures of the S_0 and ^1L_b state could be readily optimized, the obtained minimum-energy ^1L_a structure turned out to be a first-order saddle point on the S_1 state potential energy surface from the vibrational analysis. We found one imaginary in-plane mode with main contributions from C(2)–N(1) and C(2)–C(3) shortening and stretching which leads to the ^1L_b state minimum. All attempts to reoptimize the structure using different coordinate update step sizes led either to the same structure or to the ^1L_b minimum. We conclude that the minimum of the ^1L_a state, if present at all, is very shallow. We will come back to the imaginary in-plane mode and the saddle point in subsection 3.4.

Comparing with the CASSCF data from ref. 2, the CC2 optimized excited ^1L_b and ^1L_a states display qualitatively similar structural features. Nevertheless, noticeable disagreement up to few picometres is found when comparing individual bond lengths. The main difference in the structural changes upon electronic excitation between ^1L_b and ^1L_a states can be seen in Fig. 2. The upper sign gives the direction and magnitude of bond lengths changes for the ^1L_b (in red), the lower sign for the ^1L_a state (in blue). The changes upon excitation to the ^1L_b state are quite symmetric with respect to the *quasi* plane of symmetry, containing the long (*a*) axis of the molecule. The changes upon excitation to the ^1L_a state are

Table 1 Ground-state geometries and geometry changes of indole upon excitation to the L_a and the L_b states. Distances r and their changes are in pm; the full structures are given in the ESI.† For the numbering scheme refer to Fig. 1

	CC2/cc-pVTZ			CASSCF from Ref. 2		
	S_0	ΔL_b	ΔL_a	S_0	ΔL_b	ΔL_a
$r(N_1–C_2)$	138.2	+4.0	−3.6	137.9	+1.4	−0.3
$r(C_2–C_3)$	137.4	+0.6	+6.3	136.9	+1.5	+10.3
$r(C_3–C_9)$	143.2	−0.2	−0.9	144.5	−1.8	−3.4
$r(C_4–C_5)$	138.8	+4.6	+3.9	138.8	+5.8	−1.4
$r(C_5–C_6)$	141.0	+1.5	−2.8	141.7	+2.4	+1.3
$r(C_6–C_7)$	138.9	+3.9	+6.6	138.9	+4.5	+7.6
$r(C_7–C_8)$	139.8	+1.2	−0.6	140.5	+0.7	−1.9
$r(C_8–C_9)$	142.3	+4.0	−1.2	140.8	+5.5	+2.4
$r(N_1–C_8)$	137.8	−1.6	+3.6	137.3	−0.5	+1.8
$r(C_4–C_9)$	140.6	+0.6	+1.9	141.0	+0.9	+6.1

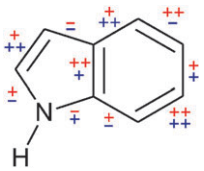

Fig. 2 Changes of the bond lengths upon electronic excitation. Upper sign (red) gives the changes upon excitation to the ^1L_b state, lower sign (in blue) for excitation to the ^1L_a state.

much more irregular, with a very large increase in bond length between the C(2) and the C(3) atoms. This coordinate has previously been postulated to be the tuning mode for the $^1L_b/^1L_a$ conical intersection by Callis.[18] ^1L_b changes show an alternating behavior for adjacent bonds, while ^1L_a changes do not.

The rotational constants of the electronic ground state of indole and their changes upon electronic excitation to the ^1L_b and ^1L_a state from the CC2 calculations are summarized in Table 2 and are compared to the experimentally determined changes of the rotational constants.[16] This analysis of the inertial parameters clearly shows, that the lowest electronically excited singlet state is the ^1L_b. None of the hitherto determined rotational constants of vibronic bands within the excited state of indole show structural ^1L_a character.[9,16]

3.1.1 Inertial axes reorientation upon electronic excitation. The geometry change upon electronic excitation causes a rotation of the inertial axes of the molecule, which can be described for a planar molecule using a single rotational angle θ_T. For indole, the *c*-axis, which is perpendicular to the aromatic plane, coincides for all three electronic states and θ_T describes the rotation of the a''-axis of the ground state into the a'-axis of the excited state about this axis.

From the *ab initio* optimized structures, the angle of reorientation of the inertial axis system upon electronic excitation θ_T can be determined using the relation for planar molecules given by Hougen and Watson:[34]

$$\tan(\theta_T) = \frac{\sum_i m_i(a_i' b_i'' - b_i' a_i'')}{\sum_i m_i(a_i' a_i'' + b_i' b_i'')} \quad (1)$$

Here, the doubly primed coordinates refer to the principal axis system in the electronic ground state and the singly primed quantities to the respective excited state inertial system and the m_i are the atomic masses. Using the CC2 optimized structures for the ^1L_b and ^1L_a states, we obtained a reorientation angle of $+0.9°$ for the ^1L_b and of $-0.6°$ for the ^1L_a state.

Table 2 Rotational constants of indole in the electronic ground state and their changes upon electronic excitation to ^1L_b and ^1L_a computed from the CC2 optimized structures using the cc-pVTZ basis set

	CC2					Experimental[16]		
	S_0	^1L_b	^1L_a	Δ^1L_b	Δ^1L_a	S_0	S_1	$S_1–S_0$
A	3880	3768	3852	−112	−28	3877.8	3743.1	−135
B	1640	1613	1605	−27	−35	1636.0	1618.1	−18
C	1152	1129	1133	−23	−19	1150.9	1130.2	−21

3.2 Vertical and adiabatic excitation energies of the ^1L_b and ^1L_a states

Table 3 gives the vertical and the adiabatic (boldface entries in the table) excitation (absorption and emission) energies of the ^1L_a and ^1L_b states of indole computed using CC2 and single point DFT/MRCI for the CC2 optimized structures. The transitions given in the table are organized as follows: the first three columns contain transitions with the ^1L_b as final or initial state, the optimized state is marked by an asterisk. The next three columns are the respective values for the ^1L_a transitions. Thus, the first column of numerical entries contains the vertical excitation energy to the ^1L_b, the second column the vertical emission energy from the ^1L_b, and the third column the adiabatic excitation energy of the ^1L_b state.

For the adiabatic excitation energies the zero-point-energy (ZPE) corrections were calculated from numerical Hessians at the CC2 level of theory for the S_0, ^1L_a and ^1L_b states, respectively. The ZPE-corrected adiabatic DFT/MRCI ^1L_b excitation energy is very close (-58 cm^{-1}) to the experimentally determined one, while CC2 shows larger deviations (+1256 cm^{-1}). The adiabatic energy gap between the ^1L_a and ^1L_b states is calculated to be 828 cm^{-1} using CC2 and to 1847 cm^{-1} at DFT/MRCI level. In the light of comparison to the experimental ^1L_b excitation energy, the latter should be the more reliable value. This energy gap of 1847 cm^{-1} should be compared to the respective value of 885 cm^{-1} for tryptamine,[22] determined at DFT/MRCI level.

We furthermore optimized the lowest triplet state of indole at the CC2 level. This state is known to have ^3L_a configuration and a geometry close to that of the ^1L_a state.[4] A DFT/MRCI single point energy calculation on the CC2 optimized structure of the lowest triplet state yields an ZPE corrected $^3L_a \leftarrow S_0$ excitation energy of 23 941 cm^{-1}. This value is in reasonable agreement with the experimental value of 24 933 cm^{-1} in an argon matrix.[35]

3.3 Permanent dipole moments and transition dipole moment orientations of the ^1L_b and ^1L_a states

The orientations of the permanent electric dipole moment in the electronic ground and the excited states and the orientations of the transition dipole moment (TDM) have been calculated using DFT/MRCI for excitation to both, ^1L_b and ^1L_a states, and compared to the experimental values.[8,16,17,36] In Table 4 the permanent dipole moments are given in Cartesian components (in Debye, D) with respect to the principal inertial axis system of the S_0 state. The TDM orientations are given as the angle θ between the projection vector of the transition dipole moment on the inertial *ab*-plane and the *a*-axis and as the angle ϕ between the TDM and the out-of-plane inertial *c*-axis:

$$\begin{aligned} \mu_a &= \mu \sin\phi \cos\theta \\ \mu_b &= \mu \sin\phi \sin\theta \\ \mu_c &= \mu \cos\phi \end{aligned} \qquad (2)$$

The values for the permanent ^1L_b dipole moments are in excellent agreement with the experimental data, both for the absolute value as well as for the components with respect to the inertial axes.

The experimentally determined transition dipole moment orientation ($\theta = +38.3^\circ$[16]) is clearly that of the ^1L_b state, with very good numerical agreement with the DFT/MRCI values ($\theta = +40^\circ$), while the ^1L_a TDM in-plane angle is calculated with the opposite sign ($\theta = -37^\circ$). The experimental value for the TDM orientation of the ^1L_b state is known very accurately from rotationally resolved electronic spectroscopy[16] and for the permanent ^1L_b dipole moment from Stark experiments in a molecular beam[17], while the transition dipole moment orientation of the ^1L_a state is much less accurately known from linear dichroism measurements on molecules partially oriented in a stretched polyethylene host.[8] Also the permanent dipole moment of the ^1L_a state, determined from Stark absorption spectroscopy of indole doped into a polymethylmethacrylate film, is less accurately known than the respective value for the ^1L_b state.

We summarize the results on the permanent dipole moments and the transition dipole moments of the ^1L_a and the ^1L_b state by stating that both properties are excellently described by the DFT/MRCI method. The numbers from CC2 do not agree with experiment to the very same extent. But the data are quite sufficiently in accord, and nothing essential changes if we deduce the above findings about indole molecular properties solely at the CC2 level of theory.

3.4 The conical intersection between ^1L_b and ^1L_a

The geometry of indole at the conical intersection between the ^1L_b and ^1L_a states was optimized at the (10,9)-CASSCF level of theory with the 6-311G(d,p) basis set. According to the CASSCF calculations, the conical intersection is located close to a linearly interpolated path between the ^1L_b and ^1L_a minima, as is the case for tryptamine.[22] Unfortunately, the excitation energies are severely overestimated by CASSCF treatment due to the neglect of dynamic electron correlation. We therefore also calculated a linearly interpolated path between our CC2 optimized ^1L_b and ^1L_a state geometries. This path is shown in Fig. 3. The predicted conical intersection in indole at the DFT/MRCI level is located more than

Table 3 Calculated vertical and adiabatic (boldface) singlet excitation and emission energies ΔE (cm^{-1}) of indole. All adiabatic excitation energies are zero-point-energy corrected. The zero-point energy correction was obtained at the CC2 level of theory with the cc-pVTZ basis. An asterisk attached to a state label is used to indicate that this state's geometry was optimized for obtaining the energies in the respective column. For vertical transition energies, thus only one of the involved states has an asterisk

Transition	$^1L_b \leftarrow S_0^*$	$S_0 \leftarrow {}^1L_b^*$	$^1L_b^* \leftarrow S_0^*$	$^1L_a \leftarrow S_0^*$	$S_0 \leftarrow {}^1L_a^*$	$^1L_a^* \leftarrow S_0^*$	$^1L_a^* \leftarrow {}^1L_b^*$
CC2	39 269	35 109	**36 496**	41 385	36 287	**37 324**	828
DFT/MRCI	37 210	33 030	**35 173**	40 179	33 885	**37 020**	1847
Experimental	—	—	**35 231**	—	—	—	—

Table 4 Permanent dipole moment: projections μ_i ($i = a, b$) onto the inertial a and b axes, and absolute values $\mu = |\vec{\mu}|$ in Debye (D). Transition dipole moment: angle θ between the projection of the TDM vector onto the ab-plane and the a-axis, and the angle ϕ between the TDM and the c-axis

	Permanent dipole moment			Transition dipole moment	
Indole	$\lvert\mu_a\rvert$	$\lvert\mu_b\rvert$	μ	θ	ϕ
exp. S_0	1.38	1.40	1.96[17]		
exp. ^1L_b	1.56	1.01	1.86[17]	+38.3[16]	+90
exp. ^1L_a			5.86[36]	−46[8]	+90
calc. S_0 DFT/MRCI	1.45	1.51	2.09		
calc. ^1L_b DFT/MRCI	1.65	1.11	1.99	+40	+90
calc. ^1L_a DFT/MRCI	5.54	1.76	5.82	−37	+90
calc. S_0 CC2	1.52	1.65	2.24		
calc. ^1L_b CC2	1.85	1.14	2.17	+55	+90
calc. ^1L_a CC2	5.53	1.33	5.69	− 46	+90

2000 cm^{-1} above the ^1L_b minimum and very close to the ^1L_a minimum. Since our DFT/MRCI path is not the true minimum energy path, this value is only an upper limit for the energy difference. The CI connecting the ^1L_a and ^1L_b states in indole lies significantly higher than the ^1L_b minimum. A perturbative approach for the description of the nonadiabatic coupling between these two states thus can be justified. We calculated how the linear path connecting the ^1L_b and ^1L_a geometries is composed from walks along individual normal modes. Here, many in-plane modes contribute, but the largest coefficient is found for mode 27 (*cf*. Table 5 in section 3.5).

The gradient difference and the derivative coupling vectors, obtained at the (10,9)-CASSCF level of theory with the

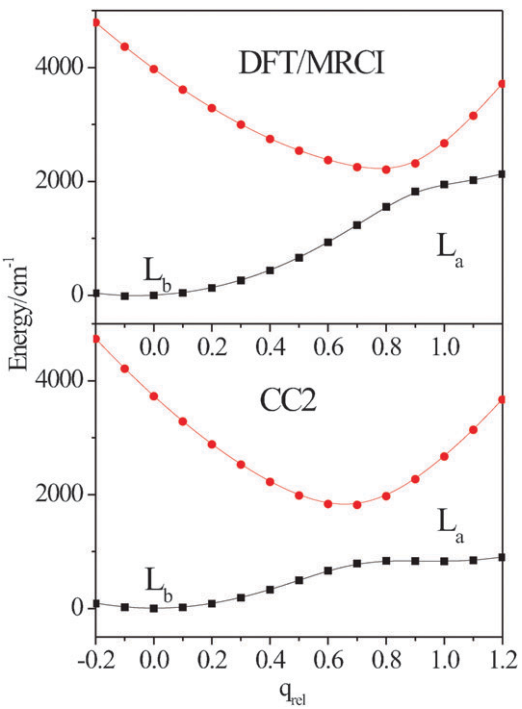

Fig. 3 One-dimensional cut through the adiabatic multidimensional potential energy surfaces of the S_1 (black squares) and S_2 (red circles) states of indole computed at the DFT/MRCI and CC2 level of theory, along a coordinate connecting the ^1L_b and ^1L_a minima, along which the conical intersection of these two surfaces is located. See the text for further details.

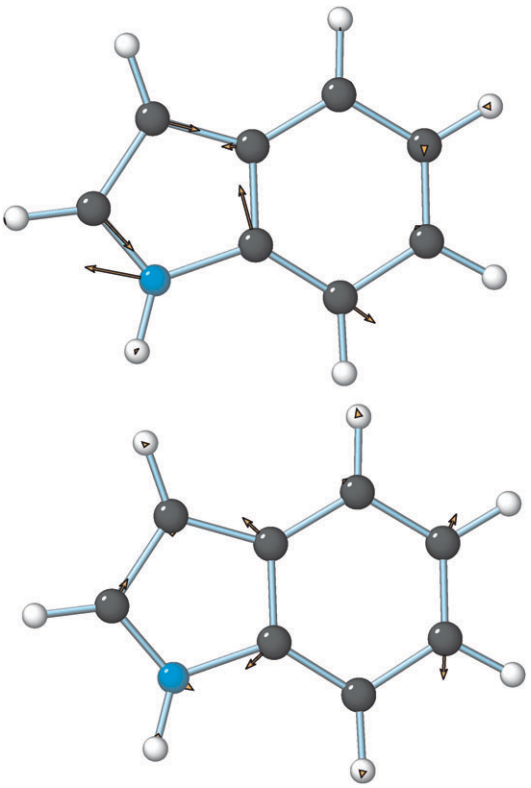

Fig. 4 Gradient difference (top) and derivative coupling vectors (bottom) of the optimized point on the CI (computed at the (10,9)-CASSCF level employing 6-311G(d,p) basis sets).

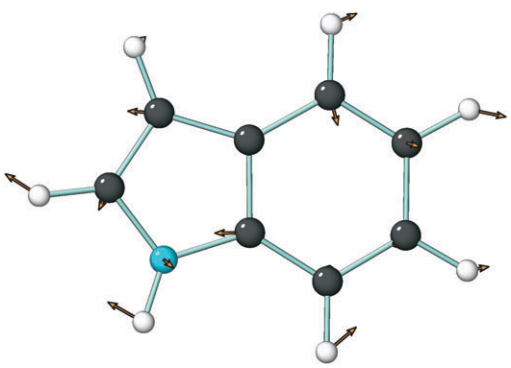

Fig. 5 Displacement vectors of the imaginary normal mode at the first-order saddle point of the ^1L_a state.

Table 5 Calculated vibrational wavenumbers in the ground and electronically excited ^1L_b states in cm^{-1} from CC2 calculations with the cc-pVTZ basis set. The first column gives the mode numbering for the ground state,[14] the last column the respective projection of the ^1L_b state modes on the ground state modes according to the Dushinsky matrix; see text for details

		S_0		^1L_b		
Mode	Sym.	Calc.	Obs.[a]	Calc.	Obs.[b]	Dushinsky
Q''_{42}	a''	215	208	170	158	$Q'_{42}(L_b) = 0.97Q''_{42}(S_0)$
Q''_{41}	a''	242	240	194	183	$Q'_{41}(L_b) = 0.95Q''_{41}(S_0)$
Q''_{29}	a'	392	400	379	379	$Q'_{29}(L_b) = 0.99Q''_{29}(S_0)$
Q''_{40}	a''	395	400	438	425	$Q'_{38}(L_b) = 0.58Q''_{40}(S_0) + 0.44Q''_{33}(S_0)$
Q''_{39}	a''	423	428	290	278	$Q'_{40}(L_b) = 0.93Q''_{39}(S_0)$
Q''_{28}	a'	541	544	477	455/480	$Q'_{28}(L_b) = 0.96Q''_{28}(S_0)$
Q''_{38}	a''	572	575	379	388	$Q'_{39}(L_b) = 0.92Q''_{38}(S_0)$
Q''_{27}	a'	605	608	563	539	$Q'_{27}(L_b) = 0.96Q''_{27}(S_0)$
Q''_{37}	a''	612	625	505	500	$Q'_{36}(L_b) = 0.93Q''_{37}(S_0)$
Q''_{36}	a''	709	715	609	—	$Q'_{34}(L_b) = 0.54Q''_{36}(S_0) + 0.47Q''_{31}(S_0)$
Q''_{35}	a''	740	738	651	—	$Q'_{32}(L_b) = 0.59Q''_{33}(S_0) + 0.48Q''_{32}(S_0)$
Q''_{34}	a''	751	762	568	—	$Q'_{35}(L_b) = 0.63Q''_{34}(S_0) + 0.54Q''_{32}(S_0)$
Q''_{26}	a'	765	761	722	718/720	$Q'_{26}(L_b) = 0.97Q''_{26}(S_0)$
Q''_{33}	a''	831	800	787	—	$Q'_{30}(L_b) = 0.80Q''_{33}(S_0) + 0.39Q''_{35}(S_0)$
Q''_{32}	a''	836	860	487	—	$Q'_{37}(L_b) = 0.27Q''_{32}(S_0) + 0.63Q''_{40}(S_0)$
Q''_{25}	a'	879	869	858	852	$Q'_{24}(L_b) = 0.91Q''_{25}(S_0)$
Q''_{24}	a'	899	900	776	784	$Q'_{25}(L_b) = 0.86Q''_{24}(S_0)$
Q''_{31}	a''	907	930	634	—	$Q'_{33}(L_b) = 0.75Q''_{31}(S_0) + 0.40Q''_{32}(S_0)$
Q''_{30}	a''	935	968	774	—	$Q'_{31}(L_b) = 0.86Q''_{30}(S_0)$
Q''_{23}	a'	1025	1015	927	909	$Q'_{23}(L_b) = 0.87Q''_{23}(S_0)$
Q''_{22}	a'	1079	1068	996	—	$Q'_{22}(L_b) = 0.62Q''_{22}(S_0) + 0.44Q''_{23}(S_0)$
Q''_{21}	a'	1107	1082	1044	1060	$Q'_{21}(L_b) = 0.81Q''_{21}(S_0)$
Q''_{20}	a'	1138	1122	1086	1086	$Q'_{20}(L_b) = 0.77Q''_{20}(S_0) + 0.58Q''_{22}(S_0)$
Q''_{19}	a'	1166	1150	1135	1111	$Q'_{19}(L_b) = 0.89Q''_{19}(S_0)$
Q''_{18}	a'	1219	1205	1180	—	$Q'_{18}(L_b) = 0.81Q''_{18}(S_0)$
Q''_{17}	a'	1259	1245	1224	—	$Q'_{17}(L_b) = 0.93Q''_{17}(S_0)$
Q''_{16}	a'	1300	1275	1273	—	$Q'_{16}(L_b) = 0.91Q''_{16}(S_0)$
Q''_{15}	a'	1370	1300	1319	—	$Q'_{15}(L_b) = 0.74Q''_{15}(S_0) + 0.53Q''_{14}(S_0)$
Q''_{14}	a'	1409	1348	1357	—	$Q'_{14}(L_b) = 0.60Q''_{14}(S_0) + 0.56Q''_{15}(S_0)$
Q''_{13}	a'	1456	1410	1392	—	$Q'_{13}(L_b) = 0.54Q''_{13}(S_0) + 0.47Q''_{12}(S_0)$
Q''_{12}	a'	1499	1458	1628	—	$Q'_{12}(L_b) = 0.52Q''_{12}(S_0) + 0.60Q''_{9}(S_0)$
Q''_{11}	a'	1509	1489	1423	—	$Q'_{11}(L_b) = 0.65Q''_{11}(S_0) + 0.50Q''_{10}(S_0)$
Q''_{10}	a'	1536	1510	1432	—	$Q'_{10}(L_b) = 0.70Q''_{19}(S_0) + 0.47Q''_{11}(S_0)$
Q''_{9}	a'	1606	1578	1628	—	$Q'_{9}(L_b) = 0.60Q''_{9}(S_0) + 0.52Q''_{12}(S_0)$
Q''_{8}	a'	1655	1617	1555	—	$Q'_{8}(L_b) = 0.77Q''_{8}(S_0)$
Q''_{7}	a'	3193	3068	3200	—	$Q'_{7}(L_b) = 0.77Q''_{7}(S_0)$
Q''_{6}	a'	3200	3068	3214	—	$Q'_{6}(L_b) = 0.84Q''_{6}(S_0)$
Q''_{5}	a'	3212	3068	3226	—	$Q'_{5}(L_b) = 0.82Q''_{5}(S_0)$
Q''_{4}	a'	3223	3083	3237	—	$Q'_{4}(L_b) = 0.89Q''_{4}(S_0)$
Q''_{3}	a'	3267	3083	3265	—	$Q'_{3}(L_b) = 0.85Q''_{3}(S_0)$
Q''_{2}	a'	3285	3140	3303	—	$Q'_{2}(L_b) = 0.85Q''_{2}(S_0)$
Q''_{1}	a'	3672	3520	3627	—	$Q'_{1}(L_b) = 1.00Q''_{1}(S_0)$

[a] Ground state frequencies from ref. 38. [b] Excited state frequencies from ref. 39; the a'' frequencies are calculated from the experimental overtone wavenumbers assuming harmonic behavior.

6-311G(d,p) basis set, are shown in Fig. 4. The gradient difference vector represents the tuning coordinate along which the energy difference of the two states connected by the CI is modulated. Together with the derivative coupling vector, which describes the interaction of the two states, it forms the 2D branching space.[37] The main contributions to the tuning vector are located in the pyrrole moiety. A distinct shortening of the bond lengths N(1)C(2) and C(8)C(9) is accompanied by a bond stretching of C(2)C(3). The C(2)C(3) displacement was described to be the main contribution to the tuning mode by Callis [18] on the basis of the differences of π-bond orders between ^1L_a and ^1L_b states. The interstate derivative coupling vector, which is shown in the lower trace of Fig. 4 is mainly located in the benzene moiety and symmetrically distorts the six-ring about bonds C(5)C(6) and C(8)C(9). This vector strongly resembles mode Q_9, along which the gradient of the electronic transition moment is largest (*cf.* Table 6). Mode Q_9 in the excited L_b state is composed of nearly equal contributions of Q_9 and Q_{12} ground state modes (*cf.* Dushinsky decomposition in Table 5), all of which have large TDM derivatives.

For tryptamine the DFT/MRCI calculations predicted a very shallow ^1L_a minimum, so that zero-point motion alone is sufficient to completely couple ^1L_a and ^1L_b levels in the region of the ^1L_a origin.[22] As described in subsection 3.1 the optimization of the ^1L_a state of indole led to a first-order saddle point. Fig. 5 shows the displacement vectors of the imaginary mode from the normal mode analysis at the CC2 level at the saddle point geometry. An optimization starting from this geometry displaced along the mode with negative curvature of the PES converged to the ^1L_b geometry. According to Fig. 3, the ^1L_a state minimum (if it exists at all) will be located rather close to the CI. Then, in order to funnel from this ^1L_a structure through the CI into the ^1L_b state, the system needs to overcome only a very shallow barrier, which should be possible already due to zero-point motion. Alternatively, one may suspect that our CC2 optimized ^1L_a geometry is itself a point on the CI if the latter displays an avoided crossing like that which appears at the CC2 level of theory. In this case, the imaginary mode from the frequency analysis at the CC2 level should exhibit some similarity with the gradient difference or derivative coupling vectors shown in Fig. 4. We did not, however, further investigate this aspect.

3.5 Franck–Condon–Herzberg–Teller simulation of the ^1L_b vibronic spectrum of indole

Table 5 shows the results of a normal mode analysis for the ground and the excited ^1L_b state. For the numbering, the modes are grouped by symmetry and then sorted by

Table 6 Calculated vibrational frequencies in cm^{-1} for the electronically excited ^1L_b state from CC2 calculations (cc-pVTZ basis set) along with the moduli of the TDM derivatives from the DFT/MRCI calculations $|(\partial\vec{\mu}_{mn}/\partial Q'_i)_{\mathbf{Q}'=0}|$ in $ea_0/\text{Å(u)}^{1/2}$, the Franck–Condon (FC) contributions $\vec{\mu}_{mn}(\mathbf{Q}'=0)\langle\mathbf{v}''_{(m)}|\mathbf{v}'_{(n)}\rangle$, Herzberg–Teller (HT) contributions $\sum_i(\partial\vec{\mu}_{mn}/\partial Q'_i)_{\mathbf{Q}'=0}\langle\mathbf{v}''_{(m)}|Q'_i|\mathbf{v}'_{(n)}\rangle$ in Cartesian components and moduli. Resulting polar angles θ and ϕ of the TDM with the main inertial axes are given for each transition

No.	Sym.	lit. [14]	^1L_b	$\lvert\partial\vec{\mu}/\partial Q'\rvert$	FC$_x$	FC$_y$	FC$_z$	|FC|	HT$_x$	HT$_y$	HT$_z$	|HT|	θ	ϕ
1	a″	Q'_{42}	170	0.0032	0.0001	−0.0001	0.0000	0.0002	0.0001	−0.0002	−0.0003	0.0003	64	28
2	a″	Q'_{41}	194	0.0050	0.0000	0.0000	0.0000	0.0000	0.0000	0.0003	0.0004	0.0005	69	1
3	a″	Q'_{40}	290	0.0077	0.0000	0.0000	0.0000	0.0000	0.0001	0.0008	0.0007	0.0010	81	6
4	a′	Q'_{29}	379	0.1892	0.0400	−0.0444	0.0000	0.0598	0.0326	−0.0682	0.0000	0.0756	65	90
5	a″	Q'_{39}	379	0.0322	0.0012	−0.0013	0.0000	0.0018	0.0009	−0.0024	0.0032	0.0041	32	19
6	a″	Q'_{38}	438	0.0359	0.0000	0.0000	0.0000	0.0000	0.0000	−0.0002	0.0035	0.0035	−5	0
7	a′	Q'_{28}	477	0.6262	−0.0071	0.0079	0.0000	0.0107	−0.0433	−0.0148	0.0000	0.0458	−40	90
8	a″	Q'_{37}	487	0.0023	0.0000	0.0000	0.0000	0.0000	0.0000	0.0001	0.0015	0.0015	40	1
9	a″	Q'_{36}	505	0.0640	0.0000	0.0000	0.0000	0.0000	0.0000	0.0000	−0.0023	0.0023	16	0
10	a′	Q'_{27}	563	0.5097	0.0807	−0.0894	0.0000	0.1205	0.0803	−0.1338	0.0000	0.1560	63	90
11	a″	Q'_{35}	568	0.0463	0.0000	0.0000	0.0000	0.0000	−0.0001	−0.0004	0.0047	0.0047	88	1
12	a″	Q'_{34}	609	0.0536	0.0000	0.0000	0.0000	0.0000	0.0000	−0.0002	−0.0071	0.0071	48	0
13	a″	Q'_{33}	634	0.0236	0.0000	0.0000	0.0000	0.0000	−0.0001	−0.0004	−0.0019	0.0020	63	1
14	a″	Q'_{32}	651	0.0118	0.0000	0.0000	0.0000	0.0000	0.0002	0.0009	−0.0019	0.0021	−22	0
15	a′	Q'_{26}	722	0.3087	0.1427	−0.1583	0.0000	0.2131	0.1147	−0.1815	−0.0001	0.2147	42	90
16	a″	Q'_{31}	774	0.0152	−0.0001	0.0001	0.0000	0.0002	−0.0068	−0.0322	0.0001	0.0329	−41	8
17	a′	Q'_{25}	776	0.5419	0.0129	−0.0143	0.0000	0.0193	0.0113	−0.0159	−0.0025	0.0196	−62	90
18	a″	Q'_{30}	787	0.0009	0.0000	0.0000	0.0000	0.0000	0.0000	0.0001	−0.0010	0.0010	−36	2
19	a′	Q'_{24}	858	0.2008	0.0343	−0.0380	0.0000	0.0512	0.0430	−0.0359	0.0000	0.0561	75	90
20	a′	Q'_{23}	927	0.4174	−0.0514	0.0570	0.0000	0.0767	−0.0729	0.0847	0.0001	0.1117	62	90
21	a′	Q'_{22}	996	0.4217	0.1244	−0.1380	0.0000	0.1858	0.0871	−0.1322	−0.0001	0.1584	48	90
22	a′	Q'_{21}	1045	0.1070	0.0057	−0.0063	0.0000	0.0085	0.0087	0.0010	0.0000	0.0088	89	90
23	a′	Q'_{20}	1086	0.1256	−0.0077	0.0085	0.0000	0.0115	0.0066	0.0034	0.0000	0.0074	34	90
24	a′	Q'_{19}	1135	0.1903	−0.0006	0.0007	0.0000	0.0009	0.0064	0.0195	0.0001	0.0205	−74	90
25	a′	Q'_{18}	1180	0.2115	−0.0085	0.0094	0.0000	0.0127	−0.0045	0.0280	0.0000	0.0283	−51	90
26	a′	Q'_{17}	1224	0.1281	0.0038	−0.0042	0.0000	0.0057	0.0164	−0.0053	0.0000	0.0173	−69	90
27	a′	Q'_{16}	1273	0.3105	0.0373	−0.0413	0.0000	0.0556	0.0536	−0.0579	0.0000	0.0790	44	90
28	a′	Q'_{15}	1320	0.2338	−0.0742	0.0823	0.0000	0.1108	−0.0836	0.1033	0.0001	0.1329	50	90
29	a′	Q'_{14}	1357	0.3397	−0.0453	0.0502	0.0000	0.0676	−0.0571	0.0805	0.0000	0.0987	37	90
30	a′	Q'_{13}	1392	0.0302	0.0318	−0.0352	0.0000	0.0474	0.0297	−0.0371	0.0000	0.0476	52	90
31	a′	Q'_{12}	1423	0.2754	−0.0247	0.0274	0.0000	0.0369	−0.0326	0.0091	0.0000	0.0339	66	90
32	a′	Q'_{11}	1432	0.7927	−0.0283	0.0314	0.0000	0.0422	0.0312	0.0311	0.0000	0.0440	−33	90
33	a′	Q'_{10}	1465	0.8163	0.0361	−0.0401	0.0000	0.0540	0.0549	−0.0227	0.0000	0.0594	−21	90
34	a′	Q'_{9}	1555	1.2050	0.0004	−0.0004	0.0000	0.0005	−0.0611	0.0111	0.0000	0.0620	7	90
35	a′	Q'_{8}	1629	0.6518	−0.0138	0.0153	0.0000	0.0206	−0.0191	−0.0053	0.0000	0.0198	−64	90
36	a′	Q'_{7}	3200	0.0604	−0.0002	0.0002	0.0000	0.0003	−0.0002	−0.0046	0.0000	0.0046	−14	90
37	a′	Q'_{6}	3214	0.1704	0.0033	−0.0037	0.0000	0.0050	0.0153	−0.0010	0.0000	0.0154	4	90
38	a′	Q'_{5}	3226	0.1061	−0.0037	0.0041	0.0000	0.0055	−0.0092	0.0003	0.0000	0.0092	4	90
39	a′	Q'_{4}	3237	0.0327	0.0102	−0.0113	0.0000	0.0153	0.0081	−0.0113	0.0000	0.0139	58	90
40	a′	Q'_{3}	3265	0.0481	0.0013	−0.0014	0.0000	0.0019	0.0007	−0.0051	0.0000	0.0051	76	90
41	a′	Q'_{2}	3303	0.0939	0.0071	−0.0079	0.0000	0.0106	0.0048	−0.0142	0.0000	0.0150	70	90
42	a′	Q'_{1}	3627	0.0852	−0.0020	0.0022	0.0000	0.0029	−0.0018	−0.0035	0.0000	0.0039	71	90

descending wavenumbers, first the out-of-plane modes numbered from Q_{42} to Q_{30}, followed by the in-plane modes from Q_{29} to Q_1. The vibrational modes given in Table 5 are sorted by ascending frequencies of the calculated S_0 vibrations. Special care must be taken for the ^1L_b state, since the energetic ordering of the modes changes and accordingly the numbering. The four lowest-wavenumber in-plane (a′) modes $Q'_{29} - Q'_{26}$ are depicted in Fig. 6. The calculated wavenumbers for both states are compared to the experimental ground state[38] and ^1L_b frequencies[39] in Table 5. The last column gives the composition of the excited state mode from the ground state modes. Only elements with a contribution of 0.4 or larger have been taken from the full Dushinsky matrix and have been used to make the assignments of excited state to ground state modes. Based on this Dushinsky matrix we performed the assignments of the excited state vibrations to the respective ground state vibrations. Based on symmetry and normal mode frequencies, the assignments to the experimental frequencies is in general rather straightforward. Since the ordering of the frequencies in the ground and the ^1L_b state is different, for some modes the numbering changes between these two states, *i.e.*, Q'_{25} of the ^1L_b state corresponds to Q''_{24} in the S_0 ground state.

A problem is posed by the close pair of intense transitions at 455/480 cm^{-1} since no two computed vibrations are sufficiently close to explain both bands. The most probable explanation is a Fermi resonance between the in-plane mode Q'_{28} and the combination of the out-of-plane modes Q'_{39} at 278 cm^{-1} and Q'_{41} at 183 cm^{-1} as already proposed by Barstis *et al.*[14]

The vibronic spectrum of indole was then simulated within the framework of the perturbative Herzberg–Teller formalism for vibronic coupling.[10] Within the Born–Oppenheimer approximation the vibronic wavefunction was factored in a vibrational part $\langle \mathbf{Q}|\mathbf{v}\rangle$ which depends only on a suitable vector of nuclear coordinates $\mathbf{Q}$ and an electronic part $\Psi_m(\mathbf{q},\mathbf{Q})$ which depends on the electronic coordinates $\mathbf{q}$ and parametrically on the nuclear coordinates $\mathbf{Q}$:

$$\Phi_{m\mathbf{v}}(\mathbf{q},\mathbf{Q}) = \Psi_m(\mathbf{q},\mathbf{Q})\ \langle \mathbf{Q}|\mathbf{v}\rangle \tag{3}$$

Here, m and $\mathbf{v}$ represent the electronic quantum number and the vector of vibrational quantum numbers, respectively. The transition dipole moment for a transition between an initial vibronic state $|m,\mathbf{v''}_{(m)}\rangle$ and a final vibronic state $|n,\mathbf{v''}_{(n)}\rangle$ is defined as:

$$\vec{M}_{m\mathbf{v}'',n\mathbf{v}'} = \langle \mathbf{v}''_{(m)}|\vec{\mu}_{mn}(\mathbf{Q})|\mathbf{v}'_{(n)}\rangle \tag{4}$$

with the geometry dependent electronic transition dipole moment $\vec{\mu}_{mn}(\mathbf{Q})$:

$$\vec{\mu}_{mn}(\mathbf{Q}) = \langle \Psi_m|\hat{\vec{\mu}}|\Psi_n\rangle;\ \ \hat{\vec{\mu}} = \sum_i e\hat{\vec{r}}_i \tag{5}$$

where $\hat{\vec{r}}_i$ is the position vector of the ith electron. The dependence of the electronic transition dipole moment $\vec{\mu}_{mn}(\mathbf{Q})$ on the nuclear coordinates $\mathbf{Q}$ can be approximated by expanding $\vec{\mu}_{mn}(\mathbf{Q})$ in a Taylor series about some suitable reference position $\mathbf{Q}_0$. In the practical calculations, we express the TDM as a function of the final state normal coordinates $\mathbf{Q}'$ and employ the final state equilibrium geometry ($\mathbf{Q}' = \mathbf{0}$) as the reference. Truncation of the expansion after the linear expansion term and insertion into eqn (4) yields:

$$\vec{M}_{m\mathbf{v}'',n\mathbf{v}'} = \vec{\mu}_{mn}(\mathbf{Q}'=0)\langle \mathbf{v}''_{(m)}|\mathbf{v}'_{(n)}\rangle + \sum_i \left(\frac{\partial\vec{\mu}_{mn}}{\partial Q'_i}\right)_{\mathbf{Q}'=0} \langle \mathbf{v}''_{(m)}|Q'_i|\mathbf{v}'_{(n)}\rangle \tag{6}$$

The Franck–Condon (FC) integrals $\langle \mathbf{v}''|\mathbf{v}'\rangle$ in eqn (6) were evaluated using the recursive relations of Doktorov[40]. The integrals $\langle \mathbf{v}''|Q'_i|\mathbf{v}'\rangle$ in eqn (6) can be calculated from FC integrals *via*:

$$\langle \mathbf{v}''|Q'_i|\mathbf{v}'\rangle = \sqrt{\frac{\hbar}{2\omega_i}}[\sqrt{\mathbf{v}'_i}\langle \mathbf{v}''|\mathbf{v}'_1,\ldots,(\mathbf{v}'_i-1),\ldots,\mathbf{v}'_N\rangle + \sqrt{\mathbf{v}'_i+1}\langle \mathbf{v}''|\mathbf{v}'_1,\ldots,(\mathbf{v}'_i+1),\ldots,\mathbf{v}'_N\rangle] \tag{7}$$

Displacement of the excited state geometry of the state n along normal modes Q'_i mixes so-called crude Born–Oppenheimer wavefunctions if the coupling between the states is symmetry-allowed and the states are sufficiently close to each other. Through the displacements, the excited state n may thus gain (or lose) intensity from (or to) perturbing state(s). We calculated the derivatives of the transition moments $\vec{\mu}_{mn}(\mathbf{Q})'$ with respect to the normal modes Q'_i of the ^1L_b state numerically from both DFT/MRCI and CC2 transition dipole moments of the respective state using central finite differences:

$$\left(\frac{\partial\vec{\mu}_{mn}}{\partial Q'_i}\right)_{\mathbf{Q}'=0} = \frac{\vec{\mu}_{mn}(0+\Delta_i\mathbf{1}_i) - \vec{\mu}_{mn}(0-\Delta_i\mathbf{1}_i)}{2\Delta_i} \tag{8}$$

Here, $\mathbf{1}_i$ is a unit vector pointing into the direction of normal mode i. Δ_i is a (scalar) displacement which should be chosen small enough to ensure the applicability of the linear approximation, but large enough to avoid numerical instabilities. In practice, we transform eqn (8) to dimensionless oscillator coordinates $\mathbf{q} = \left(\frac{\omega}{\hbar}\right)^{\frac{1}{2}}\mathbf{Q}$ and introduce a common displacement Δ for all normal modes. $\Delta = 0.1$ was used here.

The products $\vec{\mu}_{mn}(\mathbf{Q}'=0)\langle \mathbf{v}''_{(m)}|\mathbf{v}'_{(n)}\rangle$ and $\sum_i \left(\frac{\partial\vec{\mu}_{mn}}{\partial Q'_i}\right)_{\mathbf{Q}'=0}\left\langle \mathbf{v}''_{(m)}|Q'_i|\mathbf{v}'_{(n)}\right\rangle$ from eqn (6), and the moduli of the derivatives $|\partial\vec{\mu}_{mn}/\partial Q'_i|$ according to eqn (8) are given in Table 6 for each of the modes. Here, the labeling used is the one of the ^1L_b state, taken from the last column of Table 5.

Fig. 7 compares the simulation of the vibronic absorption spectrum of indole using the Franck–Condon approximation (upper trace) and Herzberg–Teller theory (lower trace). Since both the ground and the excited ^1L_b state have a′ symmetry, only a′-symmetric vibrations or even overtones of a″-symmetric vibrations are FC allowed. Clearly, the in-plane mode Q'_{28}, which is calculated at 477 cm^{-1} in the excited ^1L_b state (see Table 5) gains most of its oscillator strength through vibronic coupling to the ^1L_a state. This can also be seen from the large derivative of the transition dipole moment with respect to mode Q'_{28} in Table 6. Also mode 26 (calculated at 722 cm^{-1} for the ^1L_b state) gains intensity from vibronic coupling, as can be inferred from the comparison of a FCHT simulation with the FC simulation in Fig. 7 and from Table 6.

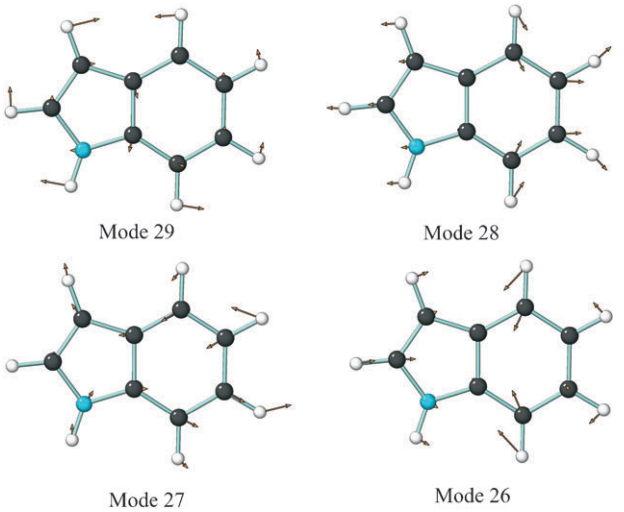

Fig. 6 Vibrational in-plane modes Q'_{29} through Q'_{26} of the ^1L_b state.

The comparison of FC and FCHT intensities with the experiment are complicated by the existence of a Fermi resonance of mode Q'_{26} with the combination of the out-of-plane modes Q'_{40} and Q'_{38}. The FC factors for the out-of-plane fundamentals are zero, as can be expected for a planar molecule, but these bands gain some intensity *via* HT coupling. *Albeit* very weak, it might be possible to detect these bands, since the analysis of the TDM angles shows, that the fundamentals of these bands will have mainly *c*-type character. The concentration of most of the bands intensity in the *Q*-branch might make their detection in a rotationally resolved electronic spectrum possible in the future, utilizing more sensitive detection devices. If these out-of-plane bands gain intensity (and band type) from HT coupling, there must be an electronic state of appropriate symmetry near-by. We propose the repulsive $\pi\sigma^*$ state, which comes from a $5a'' \rightarrow 27a'$ excitation to be the vibronically coupled state, although its oscillator strength is small. The overtones of the out-of-plane vibrations exhibit an angle ϕ of 90 degrees and therefore *ab* hybrid type for the band shape, as has been observed experimentally.[9]

Fig. 8 compares the computed vibronic spectrum with the experimental (laser induced fluorescence) spectrum.[9] Quite good agreement between the experimental and FCHT simulated absorption intensities is found, keeping in mind, that our model does not account for Fermi resonances and that the intensities of modes Q'_{27} and Q'_{26} should be divided up into two peaks. The intensities toward the blue end of the spectrum are considerably too high (both, for the FC as for the FCHT calculations, but in the latter the effect is more pronounced). This points to a deactivation path which is not considered in the present model. One plausible explanation is a crossing to a repulsive $\pi\sigma^*$ state at higher energies as proposed by Domcke and Sobolewski.[5] Tunneling through the barrier formed by the intersection of $\pi\pi^*$ and $\pi\sigma^*$ state should then decrease the lifetime of high-lying vibronic levels. Experimentally it is found, that the lifetime in the 1000 cm^{-1} region is a factor of three shorter than in the region of the electronic origin.[9]

Additionally, we simulated some of the single vibronic level fluorescence (SVLF) emission spectra of indole from the literature in the FCHT approximation. Fig. 9 shows the

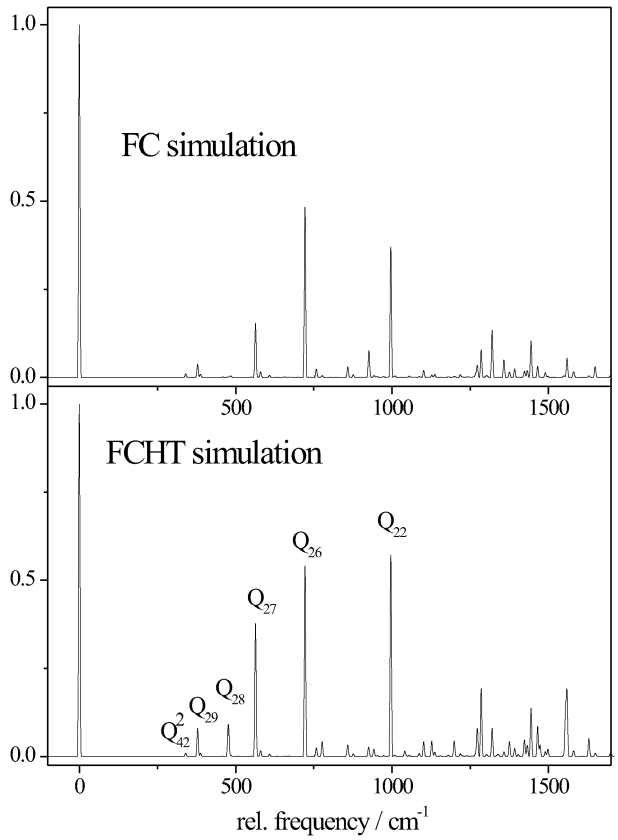

Fig. 7 Simulation of the first 1800 cm^{-1} of the absorption spectrum of the ^1L_b state using only the FC terms from eqn (6) (upper trace) and including the Herzberg–Teller terms (lower trace).

simulated and experimental emission spectrum (reconstructed from the emission spectrum[39] and the Franck–Condon factors[1]) observed *via* excitation of the vibrationless origin 0,0 of the ^1L_b state, the first overtone of mode Q'_{42} at 316 cm^{-1}, mode Q'_{27} at 540 cm^{-1}, and mode 26 at 718 cm^{-1}. Also for the emission spectrum the FCHT simulation yields qualitatively better agreement with the experiment, than a pure FC simulation (shown in the respective upper rows of Fig. 9). Nevertheless, there is still a discrepancy between the experimental and computed intensity of the bands allowed only *via* vibronic coupling.

Further investigations are underway, to clarify the reasons for these differences. At least to some extent, they may be due the truncation of the Taylor expansion in eqn (6) after the linear term. Pointwise calculations of the TDM around the equilibrium position indicate that for some of the modes higher terms of the expansion are needed. Furthermore, anharmonicities should be taken into account in particular for the excited state potential energy surfaces. As the calculations revealed that the ^1L_a state minimum energy structure is located on the adiabatic S_1 state potential energy surface not far away from the ^1L_b minimum, noticeable deviations from harmonic behavior are likely. In any case, the harmonic approximation is known to perform not overwhelmingly well for low-energy modes of complex molecules. In the extreme case, deficiencies of the perturbation theory methodology for vibronic coupling are involved.

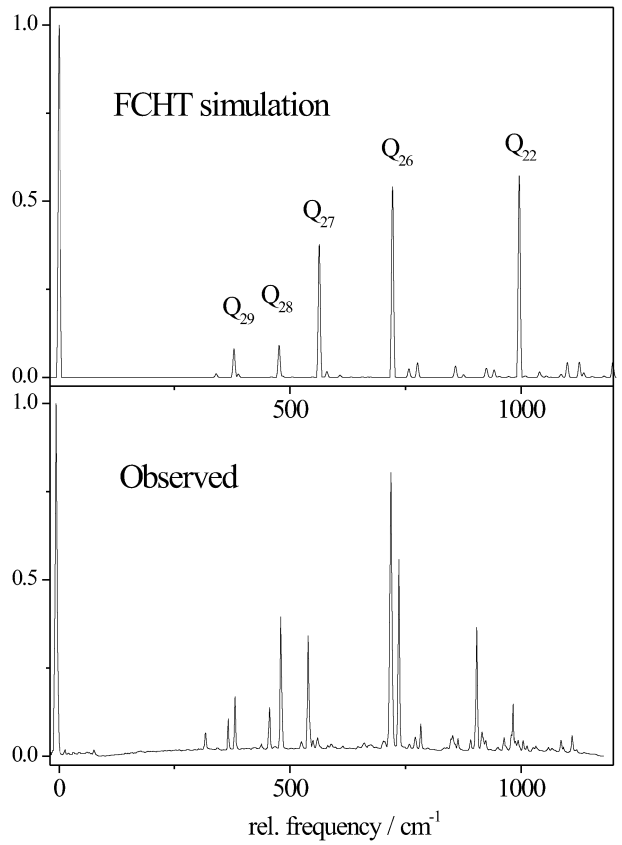

Fig. 8 Comparison of the simulation of the vibronic spectrum of the ^1L_b state using the FCHT terms from eqn (6) with the experimental spectrum.[9]

4. Conclusions

We have performed *ab initio* optimizations of the geometries of the lowest excited singlet states of indole and computed the electronic transition properties from the ground state to the excited singlet states. The ^1L_a geometry is found to be very close to the conical intersection, connecting the ^1L_a and ^1L_b state. Apparently no noticeable barrier exists between the ^1L_a state and the CI, so that pure ^1L_a states, accessed by a spectroscopic transition, will funnel directly through the CI into the ^1L_b minimum.

From the optimized geometries, the axis reorientation angles upon electronic excitation are computed to $+0.9^\circ$ and -0.6° for excitation to the ^1L_b and ^1L_a states, respectively. The adiabatic excitation energy of the ^1L_b state calculated at the DFT/MRCI level of theory, with inclusion of ZPE correction, of 35173 cm^{-1} is in very good agreement with the experimentally determined value of 35231 cm^{-1}. At the same level of theory the ^1L_a–^1L_b splitting is predicted to be 1847 cm^{-1}. This relatively large gap suggests the application of Herzberg–Teller perturbation theory for the calculation of the vibronic spectrum of indole. In contrast to the case of tryptamine, where a low-lying conical intersection efficiently couples dark vibronic levels of the ^1L_a state to the bright ^1L_b foreground state, the vibronic spectrum of indole is dominated by vibrational activity in the ^1L_b state, with vibronic perturbations of selected vibrational modes. These modes bear some resemblance to the difference vector for passing from the ^1L_b to the ^1L_a geometry. Nevertheless, also coupling to the higher lying B_a and B_b states might contribute to the vibronic coupling. While these states are energetically far away, the larger transition dipole moment can compensate for this. Using DFT/MRCI, we calculated the vertical excitation energy to the B_b state to be 6.08 eV (204 nm) and excitation to the B_a state at 6.53 eV (190 nm). The transition dipole moment vectors make an angle with the inertial *a*-axis of 18 and 33°, respectively. These values are in fair agreement with the experimental values from Albinsson and Nordén.[8] Within our numerical differentiation scheme for Herzberg–Teller coupling, the configuration interaction wavefunctions are variationally optimized in a CSF basis for each distorted geometry. The change of the configuration state vector with nuclear geometry may in principle be caused by the whole set of Russel–Saunders states, which are present in the basis. In order to break down the Herzberg–Teller activitiy into contributions from individual excited states one would need to expand the Herzberg–Teller derivatives in a sum over states. A thorough computation of this type is beyond the scope of the present publication, but will be subject of future work.

To sharpen the description of these results even more, one might say that the HT active modes drive the molecule into the conical intersection, since these modes mark the path along which both states are connected. This might be generalized; whenever there is a conical intersection on a path connecting two energetically nearby bound states, it will be the HT active modes that drive the molecule towards the CI, since it is exactly these modes, which couple the two states electronically.

Gradient difference and interstate coupling vectors for the CI of indole have been computed. While distortions due to the gradient difference vector are located in the pyrrole moiety, the interstate coupling is mediated through benzene-like vibrations of Q_9 type. This vibration has the largest gradient of the transition dipole moment and induces therefore most efficiently HT coupling. Thus, this analysis also supports our suggestion that the HT active modes are the driving force for the coupling through the CI.

The preceding conclusions from the theoretical analysis will be used in the following for making some predictions, which we will check and try to verify using high resolution electronic spectroscopy of indole. We will give a detailed description of the experimental results in the following paper.[9]

In the energy range up to about 2000 cm^{-1} the changes of the geometry measured *via* the rotational constants will indicate exclusively the ^1L_b geometry as final state.

The axis reorientation angle θ_T for excitation to the vibrationless origin of the ^1L_b state is positive, *i.e.*, it has the same sign as the TDM orientation θ. Transitions to the vibrationsless ^1L_a state are characterized by negative values for both angles, θ and θ_T. Therefore, the angles θ and θ_T have the same sign for pure electronic transitions into both, ^1L_b and ^1L_a, states. Opposite signs of θ and θ_T, which are experimentally observed,[9] are a direct indication of vibronic coupling.

Vibronic transitions in the ^1L_b ladder will show different electronic character depending on the form of the vibrational

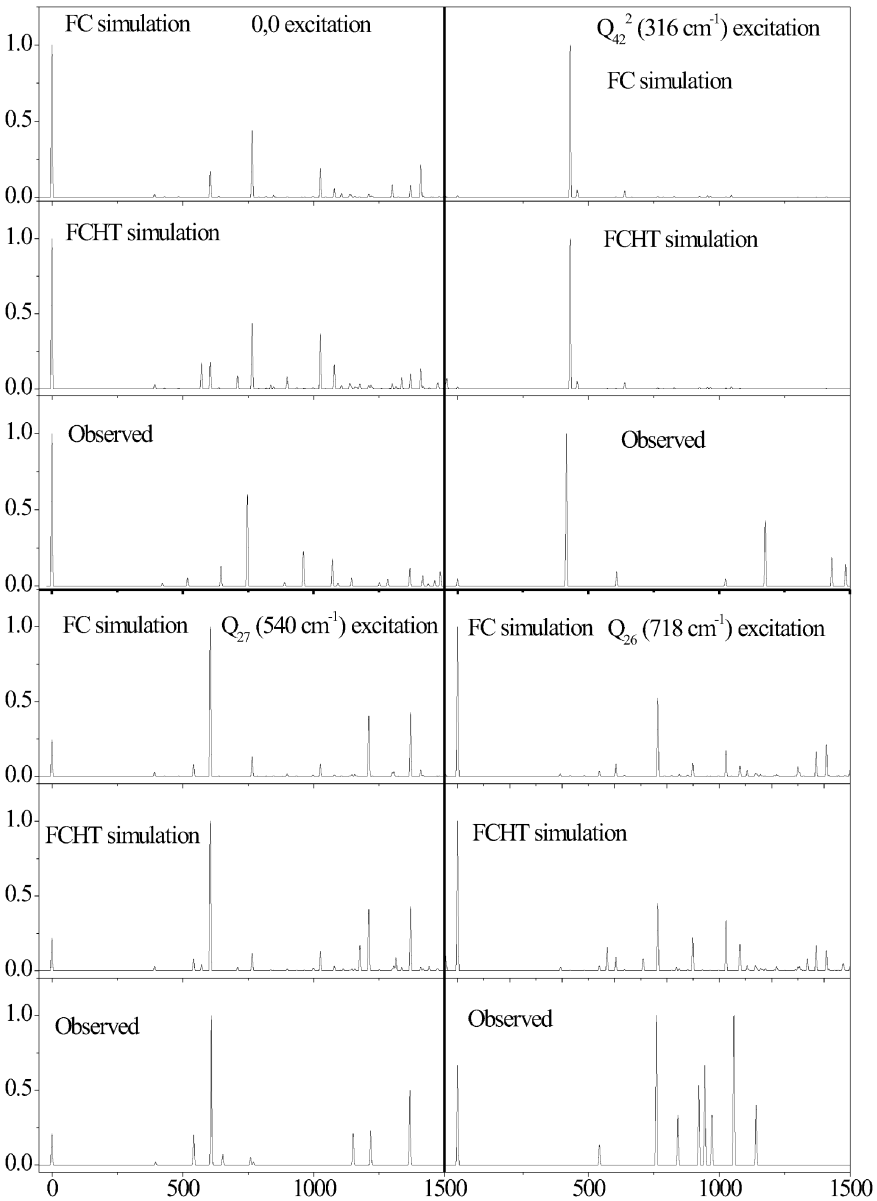

Fig. 9 Simulation of the fluorescence emission spectrum through the vibronic origin of the ^1L_b state using only the FC terms from eqn (6) and including the Herzberg–Teller terms. The other traces present emission spectra through the first overtone of mode Q'_{42} at 316 cm^{-1}, mode Q'_{27} at 540 cm^{-1}, and of mode 26 at 718 cm^{-1}.

mode and the resulting vibronic coupling strength. For instance, Q'_{28}, which is calculated at 477 cm^{-1} in the excited ^1L_b state, gains most of its oscillator strength through vibronic coupling to the ^1L_a state and will, accordingly, show a TDM orientation which is dominated by ^1L_a character.

Since the ^1L_a state exhibits no minimum along the path connecting it to the ^1L_b state, there is no observable vibrationless origin of this electronic state in the absorption spectrum.

Although the FC factors for excitation to the ^1L_b and ^1L_a states are zero for the out-of-plane vibrations of the planar indole molecule, these bands gain some intensity *via* HT coupling. These bands should exhibit pure *c*-type character and it should be possible to observe them in a sensitive spectrometer.

At about 2000 cm^{-1} above the ^1L_b origin a conical section with the ^1L_a state is located, which will alter the appearance of the absorption spectrum in this region considerably, similar to previous experimental observations in tryptamine.[22]

Acknowledgements

This work was performed in the SFB 663 TP A2, Universität Düsseldorf and was printed upon its demand with financial support from the Deutsche Forschungsgemeinschaft. DWP also acknowledges the continuing financial support of the U.S. National Science Foundation (CHE-0911117). We thank Christel Marian for helpful discussions. Granted computing time at Universitätsrechenzentrum Köln is gratefully acknowledged.

References

1 P. R. Callis, J. T. Vivian and L. S. Slater, *Chem. Phys. Lett*., 1995, **244**, 53.
2 L. Serrano-Andrés and B. O. Roos, *J. Am. Chem. Soc*., 1996, **118**, 185.
3 A. C. Borin and L. Serrano-Andrés, *Chem. Phys*., 2000, **262**, 253.
4 L. Serrano-Andrés and A. C. Borin, *Chem. Phys*., 2000, **262**, 267.
5 A. L. Sobolewski and W. Domcke, *Chem. Phys. Lett*., 1999, **315**, 293.
6 M. R. Eftink, *Methods Biochem. Anal*., 1991, **35**, 127.
7 J. Lakowicz, *Principles of Fluorescence Spectroscopy*, Plenum, New York, USA, 2nd edn, 1999.
8 B. Albinsson and B. Nordén, *J. Phys. Chem*., 1992, **96**, 6204.
9 J. Küpper, D. W. Pratt, W. L. Meerts, C. Brand, J. Tatchen and M. Schmitt, *Phys. Chem. Chem. Phys*., 2010, DOI: 10.1039/c001778g.
10 G. Herzberg, *Molecular Spectra and Molecular Structure, III. Electronic Spectra and Electronic Structure of Polyatomic Molecules*, van Nostrand Reinhold Company, New York, 1966.
11 J. R. Platt, *J. Chem. Phys*., 1949, **17**, 484.
12 D. M. Sammeth, S. Yan, L. H. Spangler and P. R. Callis, *J. Phys. Chem*., 1990, **94**, 7340.
13 M. R. Eftink, L. A. Selvidge, P. R. Callis and A. A. Rehms, *J. Phys. Chem*., 1990, **94**, 3469.
14 T. L. O. Barstis, L. I. Grace, T. M. Dunn and D. L. Lubman, *J. Phys. Chem*., 1993, **97**, 5820.
15 B. J. Fender, D. M. Sammeth and P. R. Callis, *Chem. Phys. Lett*., 1995, **239**, 31.
16 G. Berden, W. L. Meerts and E. Jalviste, *J. Chem. Phys*., 1995, **103**, 9596.
17 C. Kang, T. M. Korter and D. W. Pratt, *J. Chem. Phys*., 2005, **122**, 174301.
18 P. R. Callis, *J. Chem. Phys*., 1991, **95**, 4230.
19 L. S. Slater and P. R. Callis, *J. Phys. Chem*., 1995, **99**, 8572.
20 M. G. D. Nix, A. L. Devine, B. Cronin and M. N. R. Ashfold, *Phys. Chem. Chem. Phys*., 2006, **8**, 2610.
21 R. Berger, C. Fischer and M. Klessinger, *J. Phys. Chem. A*, 1998, **102**, 7157.
22 M. Böhm, J. Tatchen, D. Krügler, K. Kleinermanns, M. G. D. Nix, T. A. LeGreve, T. S. Zwier and M. Schmitt, *J. Phys. Chem. A*, 2009, **113**, 2456.
23 J. T. H. Dunning, *J. Chem. Phys*., 1989, **90**, 1007.
24 R. Ahlrichs, M. Bär, M. Häser, H. Horn and C. Kölmel, *Chem. Phys. Lett*., 1989, **162**, 165.
25 C. Hättig and A. Köhn, *J. Chem. Phys*., 2002, **117**, 6939.
26 C. Hättig, *J. Chem. Phys*., 2003, **118**, 7751.
27 A. Köhn and C. Hättig, *J. Chem. Phys*., 2003, **119**, 5021.
28 F. Weigend, A. Köhn and C. Hättig, *J. Chem. Phys*., 2002, **116**, 3175.
29 M. J. Frisch, G. W. Trucks, H. B. Schlegel, G. E. Scuseria, M. A. Robb, J. R. Cheeseman, J. A. Montgomery, Jr., T. Vreven, K. N. Kudin, J. C. Burant, J. M. Millam, S. S. Iyengar, J. Tomasi, V. Barone, B. Mennucci, M. Cossi, G. Scalmani, N. Rega, G. A. Petersson, H. Nakatsuji, M. Hada, M. Ehara, K. Toyota, R. Fukuda, J. Hasegawa, M. Ishida, T. Nakajima, Y. Honda, O. Kitao, H. Nakai, M. Klene, X. Li, J. E. Knox, H. P. Hratchian, J. B. Cross, C. Adamo, J. Jaramillo, R. Gomperts, R. E. Stratmann, O. Yazyev, A. J. Austin, R. Cammi, C. Pomelli, J. W. Ochterski, P. Y. Ayala, K. Morokuma, G. A. Voth, P. Salvador, J. J. Dannenberg, V. G. Zakrzewski, S. Dapprich, A. D. Daniels, M. C. Strain, O. Farkas, D. K. Malick, A. D. Rabuck, K. Raghavachari, J. B. Foresman, J. V. Ortiz, Q. Cui, A. G. Baboul, S. Clifford, J. Cioslowski, B. B. Stefanov, G. Liu, A. Liashenko, P. Piskorz, I. Komaromi, R. L. Martin, D. J. Fox, T. Keith, M. A. Al-Laham, C. Y. Peng, A. Nanayakkara, M. Challacombe, P. M. W. Gill, B. Johnson, W. Chen, M. W. Wong, C. Gonzalez and J. A. Pople, *GAUSSIAN 03, revision a.1*, Gaussian, Inc., Pittsburgh, PA, 2003.
30 M. J. Bearpark, M. A. Robb and H. B. Schlegel, *Chem. Phys. Lett*., 1994, **223**, 269.
31 S. Grimme and M. Waletzke, *J. Chem. Phys*., 1999, **111**, 5645.
32 A. D. Becke, *J. Chem. Phys*., 1993, **98**, 1372.
33 C. Lee, W. Yang and R. Parr, *Phys. Rev. B: Condens. Matter*, 1988, **37**, 785.
34 J. T. Hougen and J. K. G. Watson, *Can. J. Phys*., 1965, **43**, 298.
35 B. J. Fender, K. W. Short, D. K. Hahn and P. R. Callis, *Int. J. Quantum Chem*., 1999, **72**, 347.
36 E. Jalviste and N. Ohtab, *J. Chem. Phys*., 2004, **121**, 4730.
37 H. Köuppel, W. Domcke and L. Cederbaum, *Adv. Chem. Phys*., 1984, **57**, 59.
38 W. B. Collier, *J. Chem. Phys*., 1988, **88**, 7295.
39 G. A. Bickel, D. R. Demmer, E. A. Outhouse and S. C. Wallace, *J. Chem. Phys*., 1989, **91**, 6013.
40 E. V. Doktorov, I. A. Malkin and V. I. Man'ko, *J. Mol. Spectrosc*., 1977, **64**, 302.